Vortex matter in mesoscopic two-gap superconductor square

Paulo J. Pereira,[1] Liviu F. Chibotaru,[2] and Victor V. Moshchalkov[1]

[1]*INPAC-Institute for Nanoscale Physics and Chemistry, Katholieke Universiteit Leuven, Celestijnenlaan 200 D, B-3001 Leuven, Belgium*

[2]*Division of Quantum and Physical Chemistry and INPAC, Institute for Nanoscale Physics and Chemistry, University of Leuven, Celestijnenlaan 200F, B-3001 Leuven, Belgium*

(Received 29 May 2011; revised manuscript received 13 July 2011; published 4 October 2011)

In mesoscopic superconductors with low intrinsic pinning, the boundary plays the most important role in the stabilization of the vortex patterns. Especially in the case of symmetric sample shape, very distinct vortex locations inside the sample are defined, for the different vorticity states. The study of two-component superconductors with the Ginzburg-Landau equation implies the introduction of a coupling term between the two condensates, changing the linear part of the potential. This article presents the analysis of the impact of the competition between the coupling term and the geometry of confinement on the vortex patterns of thin mesoscopic square samples made from a two-gap superconductor. For a simple case presented here, it was found that the appearance of the noncomposite vortices is accompanied by an unusual shape of the component of the order parameter associated with the passive band as a function of the temperature. This shape is a distinct fingerprint for materials with noncomposite vortices.

DOI: 10.1103/PhysRevB.84.144504 PACS number(s): 74.78.Na, 74.20.De, 03.75.Lm

Vortex matter in two-component superconductors was intensively studied after the discovery of superconductivity in MgB_2[1] and the new iron-based superconductors.[2] Theoretically, many studies address the vortex behavior in different components of the superconducting condensate.[3] The concept of fractionalization of vortex (when magnetic flux is not quantized in units of the flux quantum $\Phi_0 = \frac{h}{2e}$) has been explored in bulk samples of unconventional superconductors,[4–7] and also studied for the case of two-component superconductors, and was found to be thermodynamically unstable in the bulk samples.[8,9] In two-component superconductors, these fractional vortex phases appear only when the condensates have different winding numbers (i.e., $L_1 \neq L_2$). It was also found that phases, where vortices belonging to different condensates of two-gap superconductors have different spatial positions (noncomposite vortices), have divergent energy density,[8] which is in accordance with the fact that only normal (Abrikosov) vortices have been detected in bulk samples.

Recent studies show that it is possible to have noncomposite vortices in thin mesoscopic superconductors,[10] and fractional flux vortex phases, thermodynamically stable, in a long mesoscopic cylinder[11] and a mesoscopic disk[12] (i.e., where the radius is of the order of the coherence length). For mesoscopic superconductor disks and cylinders, it was found that the T-H phase diagrams, corresponding to the intrinsic superconductivity in the two bands, generally do not coincide. More precisely, the phase diagram that corresponds to the passive band is shifted upward with respect to the phase diagram for the active band.[10,11] This displacement allows for vortex phases with different winding numbers in the two condensates and noncomposite vortices. Although, we note a major difference between long mesoscopic cylinders and thin mesoscopic disks;[10] in the latter the screening currents are negligible.

In mesoscopic superconductors, the coherence length (ξ) and the penetration length (λ) are of the same order of magnitude as the sample size. This makes the properties of the superconducting condensate strongly influenced by the geometry of the sample's boundary. At the mesoscopic scale, the vortex patterns are defined by the symmetry/geometry of the sample. Many studies with disks and polygons were made to investigate and understand the origin of various vortex patterns in mesoscopic samples.[13–22] In these studies, it was found that near the normal-superconducting phase boundary (PB) the condensate is mainly defined by the solutions of the linear Ginzburg-Landau (LGL) equation.[15,23] In experiments[23] on mesoscopic samples with low intrinsic pinning, the PB was found to consist of segments of a cusplike shape. Then, simulations were made[15,23] showing that this shape was due to periodic fluctuations of the ground-state eigenvalues, corresponding to different vorticities, with the magnetic field strength. An extension of these studies has shown that the vortex patterns near the PB, in mesoscopic samples, are mostly defined by linear combinations of a few eigenfunctions of the LGL equation. The nucleated vortices are always consistent with the symmetry of the sample and then pass into broken-symmetry phases by lowering the temperature.[24] The existence of non-negligible regions on the T-H phase diagram corresponding to symmetry-consistent vortex patterns is an important feature that distinguishes the bulk from thin mesoscopic superconductor samples.[13,24]

In this paper, the interplay between the geometry of the confinement and the coupling between the two condensates of the thin mesoscopic two-gap superconductors is investigated. Consider a square sample of size a of the order of the coherence length (ξ) and thickness d much smaller than ξ. Since the thickness of the sample is very small, the screening currents are not important, and the Ginzburg-Landau equation is reduced to a 2D case.[22,24] Thus, the GL free-energy functional is given by,[25]

$$\Delta F = \int \left[\sum_{n=1}^{2} \left(\frac{1}{2m_n} \left| \left(-i\hbar\nabla - \frac{2e}{c}\mathbf{A} \right) \Psi_n \right|^2 + \alpha_n |\Psi_n|^2 + \frac{1}{2}\beta_n |\Psi_n|^4 \right) - \gamma(\Psi_1^*\Psi_2 + \Psi_2^*\Psi_1) \right] dS, \quad (1)$$

where Ψ_1 and Ψ_2 are the two components of the superconducting order parameter (the index 1 and 2 refer to the

active and the passive band, respectively), and **A** is the vector potential related to the applied magnetic field, $\mathbf{H} = rot\mathbf{A}$. In (2), the variables $\alpha_1 = -a_1 t$ and $\alpha_2 = a_{20} - a_2 t$ (with $t \approx 1 - T/T_1$, where T_1 is the critical temperature of the active band) are the condensation energy coefficients, β_1 and β_2 are the nonlinearity coefficients, and γ is the Josephson coupling coefficient. The eigenfunctions of the one-component LGL equation with the usual boundary condition,

$$\left(-i\hbar\nabla - \frac{2e}{c}\mathbf{A}\right)^2 \phi_n = \lambda_n \phi_n, \tag{2}$$

$$\left(-i\hbar\nabla - \frac{2e}{c}\mathbf{A}\right)^2 \phi_n|_{\text{n.b.}} = 0, \tag{3}$$

(n.b. means that the equation is projected on the unit vector normal to the boundary) were used as a basis for the solutions of Eq. (1):

$$\Psi_1 = \sum_i u_i \phi_i \quad \Psi_2 = \sum_i v_i \phi_i. \tag{4}$$

Equations (2) and (3), at their turn, were solved by using the superconducting gauge approach.[13,26] Substituting (4) into (1), the GL functional is reduced to a polynomial with the decomposition coefficients c_i ($c_i \equiv u_i, v_i$):

$$\begin{aligned} \Delta F_n(c) &= \left(\alpha_n + \frac{\hbar^2}{2m_n S}\varepsilon_i\right) c_i^* c_i + \frac{\beta_n}{2} A_{kl}^{ij} c_i^* c_j^* c_k c_l, \\ \Delta F &= \Delta F_1(u) + \Delta F_2(v) - \gamma(u_i^* v_i + u_i v_i^*), \end{aligned} \tag{5}$$

with $\varepsilon_i = \lambda_i S/\hbar^2$ and

$$A_{kl}^{ij} = S\int \phi_i^* \phi_j^* \phi_k \phi_l dS, \tag{6}$$

where $S = a^2$ is the area of the sample. To simplify the problem, we rescaled the space coordinates and the expansion coefficients as in the previous publications,[10,24]

$$x \to \frac{x}{\sqrt{S}} \quad y \to \frac{y}{\sqrt{S}} \tag{7}$$

$$u_i \to \sqrt{-\frac{\tilde{\alpha}_1}{\beta_1}}\sqrt{\frac{\hbar^2}{2Sm_1}} u_i \quad v_i \to \sqrt{-\frac{\tilde{\alpha}_1}{\beta_1}}\sqrt{\frac{\hbar^2}{2Sm_1}} v_i, \tag{8}$$

and defined the LGL parameters as follows:

$$\tilde{\alpha}_n = \alpha_1 + \varepsilon_n \tag{9}$$

$$\alpha_n = -\frac{\hbar^2}{2m_1 \xi_n^2(T)}\gamma = \frac{\hbar^2}{2m_1 \xi_\gamma^2}. \tag{10}$$

Using these definitions, the GL functional is written as,

$$\begin{aligned} \Delta F_1(c) &= \left[\frac{\left(-\frac{S}{\xi_1^2} + \varepsilon_i\right)}{\tilde{\alpha}_1} c_i^* c_i + \frac{1}{2} A_{kl}^{ij} c_i^* c_j^* c_k c_l\right], \\ \Delta F_2(c) &= \left[\frac{\left(-\frac{S}{\xi_2^2} + \frac{m_1}{m_2}\varepsilon_i\right)}{\tilde{\alpha}_1} c_i^* c_i + \frac{1}{2}\frac{\beta_2}{\beta_1} A_{kl}^{ij} c_i^* c_j^* c_k c_l\right], \\ \frac{\Delta F}{\frac{\tilde{\alpha}_1^2}{\beta_1}}\frac{4m_1^2 S}{\hbar^4} &= \Delta F_1(u) + \Delta F_2(v) - \frac{S}{\xi_\gamma^2 \tilde{\alpha}_1}(u_i^* v_i + u_i v_i^*). \end{aligned} \tag{11}$$

The functional (11) was minimized using multiple tries of a nonlinear conjugated gradient method, which yielded the equilibrium distribution of the two components of the order parameter. The method described above, and more extensively in Ref. 13, is faster than the typical methods used to study this type of problem (i.e., finite difference and the finite element methods). This is achieved with the usage of a small basis set that already satisfies the boundary conditions, previously simplified by fixing the gauge. In the simulations presented in this article, a basis set of 900 functions was used to solve the LGL equation with the respective boundary condition, and a basis set of 24 functions was used to minimize the GL function. Reference 13 can be used to address the accuracy of calculations made with this basis size.

Figure 1(b) shows the calculated phase diagram for the two-gap superconductor square. For the square geometry, the case of a one-component mesoscopic superconductor was already investigated in previous publications.[24] To compare that case with the two-component case, we have reproduced its T-H phase diagram [displayed in the Fig. 1(a)] by setting $\Psi_2 = 0$. Near the T_c boundary, the condensate pattern is dominated by the LGL solution[13,15] that has the symmetry of the sample, while at lower temperatures [i.e., at larger values of $S/\xi^2(T)$] the nonlinear term starts to compete with the symmetry-conserving solutions, breaking the symmetry of the condensate order parameter. The vortex phase boundaries in the T-H diagram are shaped by this competition. If there were no nonlinear term, these boundaries would be vertical lines, which is quite different from what we see in Fig. 1(a).

For the two-component superconductors, the two condensates nucleate at different temperatures (the condensation temperature in the passive band is lower than in the active band).[25] As a result, the regions of the vortex phases in the T-H diagram are different for the two condensates.[10] The corresponding PBs in the two condensates are shifted relative to each other, so there is a "large" region [i.e., areas (a)–(g) of the diagram in Fig. 1(b)] where the two condensates have different vorticity. Figure 1(b) shows that there is an even bigger area where the two condensates have noncomposite vortices.

Novel vortex phases are clearly seen in our results. In the areas (d), (f), and (i) of the diagram presented in Fig. 1(b), there are vortex phases containing one antivortex only in one of the components of the order parameter. Some other interesting phases, represented in the areas (h) and (i) of this diagram and in Figs. 2(a) and 2(b), appear where one of the components is in a symmetry broken phase, while the other is almost in a symmetry-consistent vortex phase. These almost symmetric vortex phases correspond to a slightly deformed nucleated vortex pattern. For example, in the antivortex pattern (four separated vortices and one antivortex in the center) associated with area (i) of Fig. 1(b), the antivortex is dislocated toward a neighbor vortex, as can be seen in Fig. 3. The antivortex observed in this pattern is created from the interplay of two effects. The first is the requirement of the symmetry consistency of the order parameter distribution close to the superconducting-normal phase boundary.[14,15] The second is the confinement effect from the boundaries which stabilizes, in the case of vorticity three, in a configuration of four vortices plus one antivortex instead of

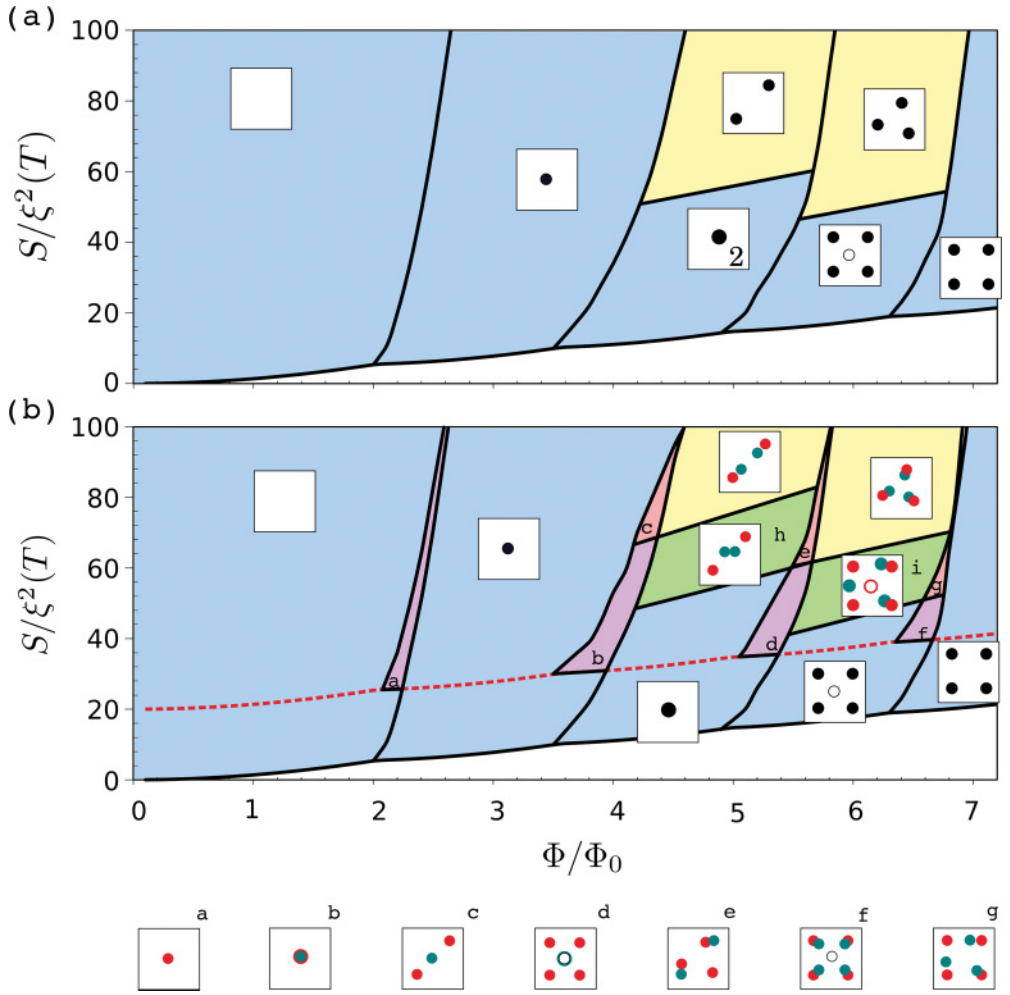

FIG. 1. (Color) Diagrams of the vortex phase boundaries for one-component (a) and two-component (b) superconductors. The one-component case is parameter free. For the two-component diagram, the values of the parameters used were $\frac{m_1}{m_2} = 1$, $\frac{\beta_2}{\beta_1} = 1$, $\frac{S}{\xi_\gamma^2} = 0.05$, and $\frac{S}{\xi_2^2(T_c)} = 20$. On the diagrams, the almost vertical lines are the boundaries for the vorticity phases, and the almost horizontal lines, inside the vorticity areas, are boundaries for the broken-symmetry phases. The dashed red line is the nucleation phase boundary for the second component with $\gamma = 0$. The small square diagrams over the regions represent the respective vortex patterns of that region. In these square diagrams, the noncomposite vortices in the active band (Ψ_1) and passive band (Ψ_2) are represented by green and red circles, respectively, and the composite vortices are represented in black as in the case of only one band on the diagram (a). The filled small circles, empty small circles, and the big filled circles correspond to vorticity 1, -1, and 2, respectively.

one giant vortex (with vorticity three) in the center. These two effects are equally present in both single-band and two-band superconductors.

Regarding the observation of noncomposite vortices in the distributions of $|\Psi_1|^2 + |\Psi_2|^2$, the total density of the superconductor condensate, we note that they are hardly seen, as shown in Fig. 2. This is due to two factors. First, the active band is typically "stronger" than the passive band, thus resulting in a higher density of the condensate. Second, the vortex cores have a radius of the order of the sample size, which is bigger than the separation between them. Although, it is difficult to distinguish the vortices of the different components in the total order parameter density distribution (lowest panel in Fig. 2). This distribution is significantly different from any of the components density distributions.

I. DEPENDENCE OF THE VORTEX DECONFINEMENT ON THE INTERBAND JOSEPHSON COUPLING AND THE CRITICAL TEMPERATURE OF THE PASSIVE BAND

We have studied the influence of the Josephson coupling (γ) and $S/\xi_2^2(T_c)$ term on the deconfinement of the vortices belonging to different condensates. We note that the vorticity regions change in the T-H phase space with the parameters γ and $S/\xi_2^2(T_c)$, and the vorticity boundaries in T-H space are functions of temperature and magnetic field. In order to analyze the problem, we took lines in the T-H space that passed through a single vorticity region. These lines were traced in different regions of the T-H diagram for different parameters, in order to compensate for the fact that vorticity regions change with these parameters. For the parameters $m_1 = m_2$, $a_1/a_2 = 1$, and $\beta_1/\beta_2 = 1$, these lines are parallel

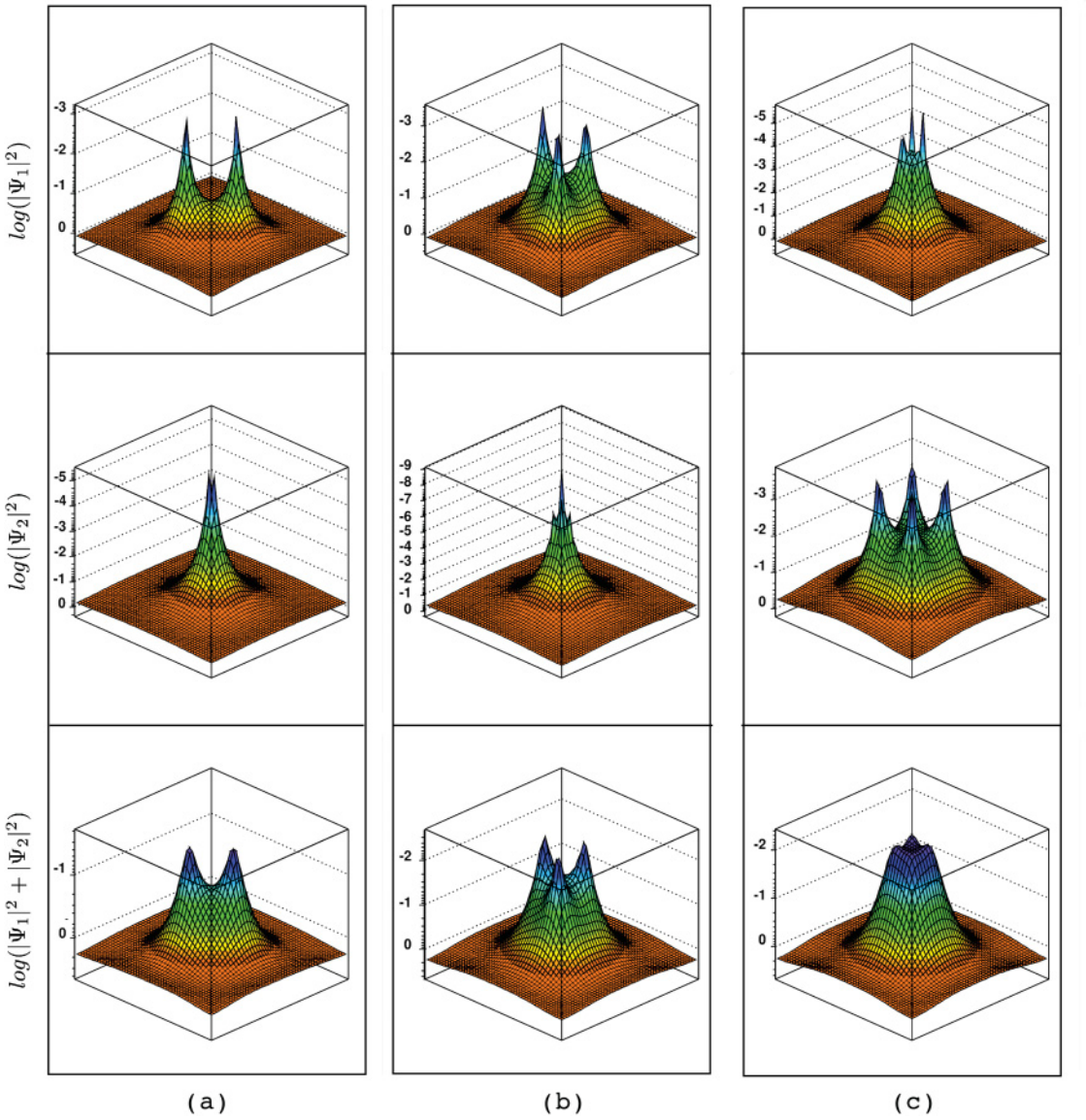

FIG. 2. (Color online) 3D view of the condensate in the common logarithm scale ($\log_{10}$). (a), (b), and (c) correspond to phases (h), (i), and (g) of the diagram 1(b) and to the parameters $(\Phi/\Phi_0, S/\xi_1^2) = (4.5, 60)$, (6, 50), and (6.6, 52), respectively. For each vertical set of plots, the top plot corresponds to $|\Psi_1|^2$, the second to $|\Psi_2|^2$, and the third to the sum. The remaining parameters are the same as in Fig. 1(b).

and they are displaced in $S/\xi_1(T)$. Simulations described at the beginning of this article were made, along the lines intercepting the two-vortex region for different values of the parameters. The displacements between these lines are listed in Table I. The results of the simulations are shown in the corresponding plots of Fig. 4, and a small diagram inside each plot shows the lines, in the T-H diagram, where the simulations where made.

The plots in Fig. 4 display the data obtained for $S/\xi_2^2(T_c) = 20$ and $S/\xi_2^2(T_c) = 100$, with the different values of S/ξ_γ^2. These plots show the $|\Psi_1|_{\rm rms}$, $|\Psi_2|_{\rm rms}$, and the distance between vortices in the two bands, in units of the sample size, as a function of $S/\xi_1(T)$. To calculate this distance in each pattern, the centers of the vortices belonging to both bands were first detected. Afterwards, the closest pair of vortices belonging to different bands was found. The distance between the two vortices of this pair is the distance shown in the plots of Fig. 4. This distance as a function of $S/\xi_1(T)^2$ reflects the difference in the transitions between the symmetry-consistent and the

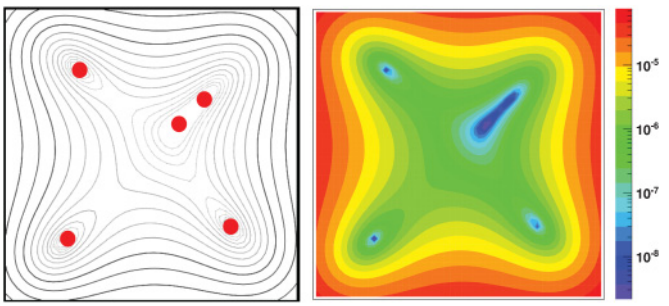

FIG. 3. (Color online) A zoom, in the center of the sample, of the passive band-density distribution for the vortex phase area (i) of Fig. 1(b).

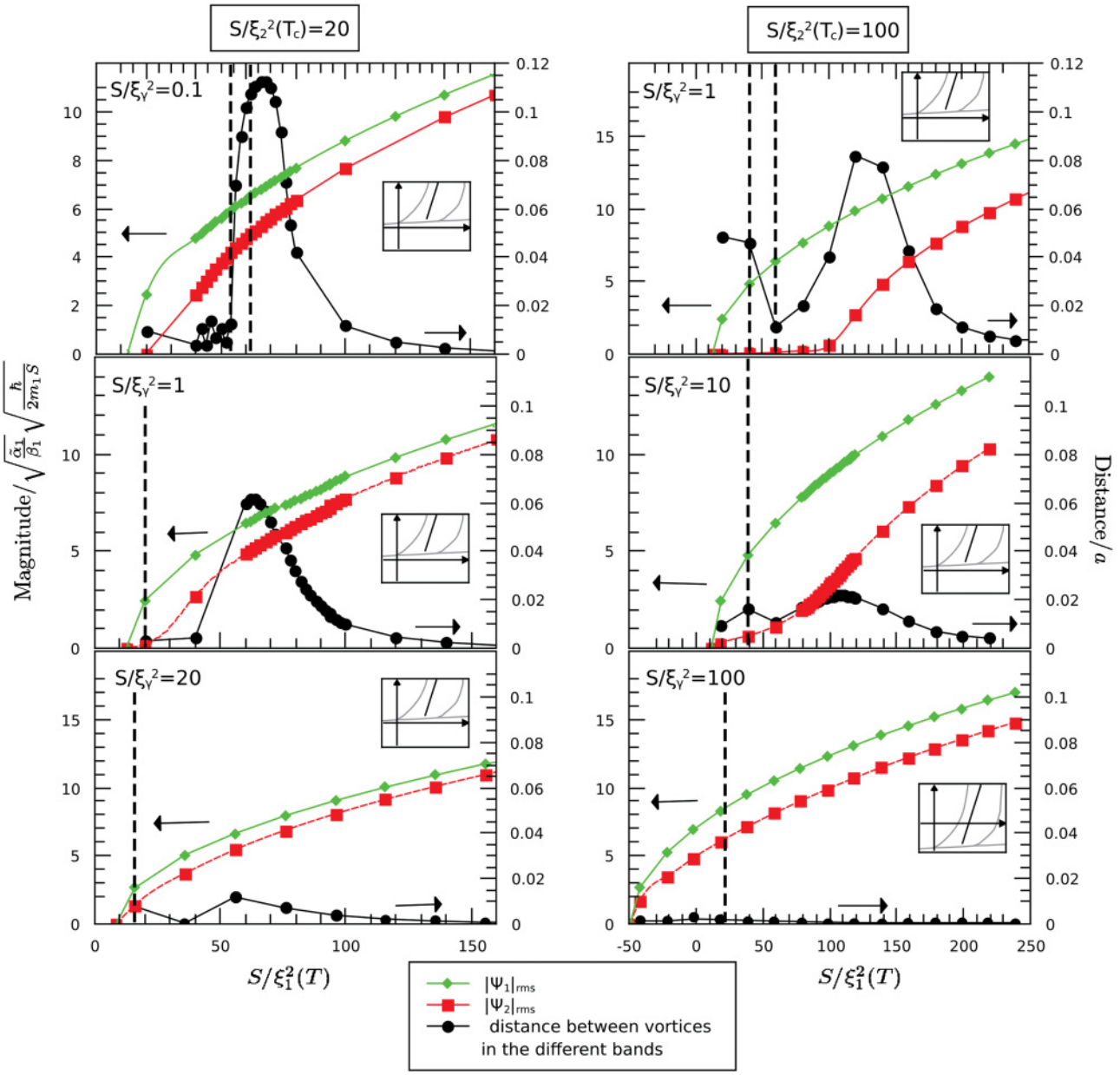

FIG. 4. (Color online) Plots of the root mean square of the two components of the order parameter, $|\Psi_1|_{\rm rms} = \sqrt{(\int |\Psi_1|^2 dS)/S}$ and $|\Psi_2|_{\rm rms} = \sqrt{(\int |\Psi_2|^2 dS)/S}$, and the distance(in units of the sample size a) between vortices in the different bands, as defined in the text, along the lines in the T-H phase space(that pass through regions of vorticity two, these lines are shown in the small plots inside the plots) for different parameters of the system. Vertical dashed lines show the transition point between symmetric and broken vortex patterns. We note that there are plots with one and plots with two vertical dashed line. In the case of one vertical line this represents the symmetry breaking of both of the condensates. In the case of two vertical lines the left and the right lines are the points were the Ψ_1 and Ψ_2 condensates break symmetry, respectively.

broken-symmetry phase in the two condensates [Fig. 1(b)]. To better compare the results obtained for different values of parameters, Table I shows the relation between these parameters and the maximum value of distance between the closest vortices in the two bands, obtained over the lines in the T-H space.

In all plots of Fig. 4, the dependence of $|\Psi_1|_{\rm rms}$ on temperature has the usual shape. However, $|\Psi_2(T)|_{\rm rms}$ strongly changes its shape as a function of γ. It has a conventional behavior corresponding to the uncoupled passive band in the case of small γ, and a conventional shape coinciding with the active band for large γ. In transition from one regime to the other, the shape of this curve has a pronounced inflection at the point of the passive band critical temperature. This inflection is due to intrinsic superconductivity in the passive band.

The shape of $|\Psi_2(T)|_{\rm rms}$, shown in the plots of Fig. 4, seems to be strongly correlated with the separation between vortices in the different bands. More precisely, different regimes,

TABLE I. Displacement of the lines on the $S/\xi_1^2(T)$-ϕ/ϕ_0 diagram [Fig. 1(b)] for which simulations in Fig. 4 were done.

Displacement	$\frac{S}{\xi_\gamma^2}$	$\frac{S}{\xi_2^2(T_c)}$	$\frac{\xi_2^2(T_c)}{\xi_\gamma}$	$\frac{d_{\max}}{a}$ [a]
0	0.1	20	0.0050	0.1124
0.5	1	20	0.0500	0.0618
4.14	10	20	0.5000	0.0119
0,	1	100	0.0100	0.0819
1	10	100	0.1000	0.0217
41.8	100	100	1.0000	0.0022

[a] $d_{\max}$ is the maximal distance found on the simulations presented in the plots of Fig. 4.

from high and low γ, seem to have a similar effect on both noncomposite vortex phenomenon and the shape of $|\Psi_2(T)|_{\rm rms}$. This means that the existence of the inflection in shape of $|\Psi_2(T)|$ can be used as a criterion of weak coupling, signaling the non-negligible vortex deconfinement effects in mesoscopic superconductors.

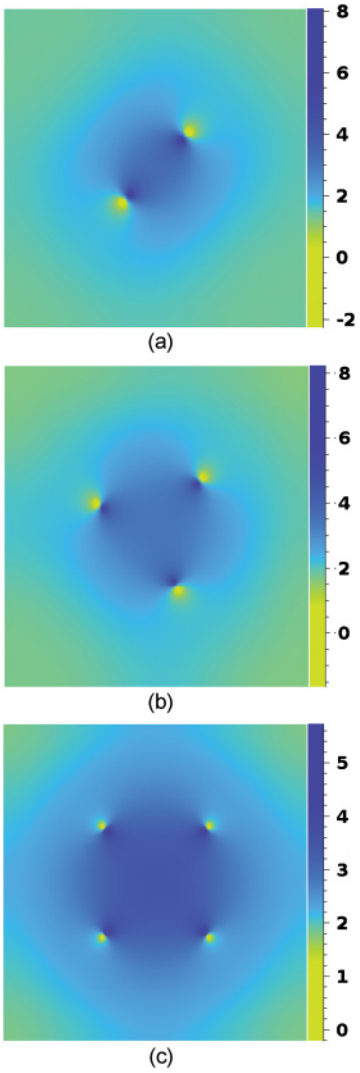

.

FIG. 5. (Color online) Density plots of the $\ln(\Psi_1/\Psi_2)$ for the MgB_2 parameters expressed in the text. The regions with the lighter green(lighter color) and darker blue(darker color for black and white picture) colors identify were Φ_1 and Φ_2 are more close to zero, respectively. (a), (b) and (c) correspond to the $\Phi/\Phi_0 = 4.5$, 6 and 7, respectively, with $\frac{S}{\xi_1^2(T)} = 100$

II. VORTEX DECONFINEMENT IN MgB_2 SAMPLES AND ITS RELATION TO THE MASS RATIO AND $\alpha_{\rm ratio}$ TERM

We have also studied a square mesoscopic sample with the parameters of MgB_2. A square sample of MgB_2 with 124×124 nm^2 area was simulated using the following MgB_2 parameters:[10] $\alpha_{\rm ratio} = 1.5$, $\beta_1/\beta_2 = 1.5$, $m_1/m_2 = 1/0.07$, $S/\xi_1^2(0) = 314.2$, $\sqrt{S}/\xi_2(T_c) = 14.35$, $\sqrt{S}/\xi_\gamma = 11.17$, and $T_c = 39$ K.

Figure 5 shows the results for some specific cases. From them we conclude that the distance between vortices in the two condensates is of the order of 2–3 nm. It is interesting to note that vortex phases that do not have a broken-symmetry phase transition also have noncomposite vortices which are very close to each other, as can be seen from Fig. 5(c). If we compare the vortex separation distances obtained in the case of the disk geometry with the present case of the square geometry for similar parameters of GL functional, we can conclude that the change of the symmetry of the sample from disk to square does not influence the vortex separation.

III. CONCLUSION

In conclusion, we have shown that lowering the symmetry of the sample's boundary from circle to square does not increase the separation of vortices in the two bands. The calculations have revealed that the phase diagram of the square is very close to the two-gap superconductor[10] disk. However, in the case of a square, a much richer phase diagram appears containing novel vortex phases. Among them we mention here one with an antivortex in only one component of the order parameter. In relation to vortex deconfinement phenomenon, we have observed that it practically disappears with the inflection point on the temperature dependence of the passive band component. This can be used as a criterion of "weak" coupling for vortex deconfinement in mesoscopic superconductors. Thus, the shape of the dependence of the passive band density $|\Psi_2|^2$ in the temperature provides a new tool for searching materials with noncomposite vortices.

As in the case of disk geometry, the visualization of the separation of vortices belonging to different condensates does not appear to be feasible for the MgB_2 samples, at least at the current technical level, due to the strong interband coupling parameter. Nevertheless we point out that the existence of such noncomposite vortices is a real mesoscopic effect, which could be observed in two-gap superconductors with a weaker coupling between the two bands.

ACKNOWLEDGMENTS

We acknowledge financial support from Methusalem Funding by the Flemish government and the SIM-GRIDPT computing center funded under project REDE/1522/RNG/2007.

[1]J. Nagamatsu, N. Nakagawa, T. Muranaka, Y. Zenitani, and J. Akimitsu, Nature (London) **410**, 63 (2001).
[2]K. Ishida, Y. Nakai, and H. Hosono, J. Phys. Soc. Jpn. **78**, 062001 (2009).
[3]A. Gurevich, Phys. Rev. B **67**, 184515 (2003); Physica C **456**, 160 (2007).
[4]M. A. Silaev, Phys. Rev. B **83**, 144519 (2011).
[5]J. R. Kirtley, P. Chaudhari, M. B. Ketchen, N. Khare, Sh.-Yu Lin, and T. Shaw, Phys. Rev. B **51**, 12057 (1995).
[6]J. Jang, D. G. Ferguson, V. Vakaryuk, R. Budakian, S. B. Chung, P. M. Goldbart, and Y. Maeno, Science **331**, 186 (2011).
[7]S. B. Chung, D. F. Agterberg, and E.-A. Kim, New J. Phys. **11**, 085004 (2009).
[8]E. Babaev, Phys. Rev. Lett. **89**, 067001 (2002); Nucl. Phys. B **686**, 397 (2004).
[9]Y. Tanaka, Phys. Rev. Lett. **88**, 017002 (2001); J. Phys. Soc. Jpn. **70**, 2844 (2001).
[10]L. F. Chibotaru, V. H. Dao, and A. Ceulemans, Europhys. Lett. **78**, 47001 (2007).
[11]L. F. Chibotaru and V. H. Dao, Phys. Rev. B **81**, 020502 (2010).
[12]R. Geurts, M. V. Milosevic, and F. M. Peeters, Phys. Rev. B **81**, 214514 (2010).
[13]L. F. Chibotaru, A. Ceuleman, M. Morelle, G. Teniers, C. Carballeira, and V. V. Moshchalkov, J. Math. Phys. **46**, 095108 (2005).
[14]L. F. Chibotaru, A. Ceulemans, V. Bruyndoncx, and V. V. Moshchalkov, Phys. Rev. Lett. **86**, 1323 (2001).
[15]L. F. Chibotaru, A. Ceulemans, V. Bruyndoncx, and V. V. Moshchalkov, Nature (London) **408**, 833 (2000).
[16]J. J. Palacios, Phys. Rev. B **58**, R5948 (1998).
[17]J. J. Palacios, Phys. Rev. Lett. **84**, 1796 (2000).
[18]A. K. Geim, I. V. Grigorieva, S. V. Dubonos, J. G. S. Lok, J. C. Maan, A. E. Filippov, and F. M. Peeters, Nature (London) **390**, 259 (1997).
[19]P. S. Deo, V. A. Schweigert, F. M. Peeters, and A. K. Geim, Phys. Rev. Lett. **79**, 4653 (1997).
[20]S. Okayasu, T. Nishio, Y. Hata, J. Suzuki, I. Kakeya, and K. Kadowaki, IEEE Trans. Appl. Supercond. **15**, 696 (2005).
[21]G. Karapetrov, J. Fedor, M. Iavarone, D. Rosenmann, and W. K. Kwok **95**, 167002 (2005).
[22]V. A. Schweigert, F. M. Peeters, and P. S. Deo, Phys. Rev. Lett. **81**, 2783 (1998); V. A. Schweigert and F. M. Peeters, Phys. Rev. B **57**, 13817 (1998).
[23]V. V. Moshchalkov, L. Gielen, C. Strunk, R. Jonckheere, X. Qiu, C. Van Haesendonck, and Y. Bruynseraede, Nature (London) **373**, 319 (1995).
[24]L. F. Chibotaru, G. Teniers, A. Ceulemans, and V. V. Moshchalkov, Phys. Rev. B **70**, 094505 (2004).
[25]M. E. Zhitomirsky and V. H. Dao, Phys. Rev. B **69**, 054508 (2004); V. H. Dao and M. E. Zhitomirsky, Eur. Phys. J. B **44**, 183 (2005).
[26]L. F. Chibotaru, A. Ceulemans, G. Teniers, V. Bruyndoncx, and V. V. Moshchalkov, Eur. Phys. J. B **27**, 341 (2002).